Transient Temperature Distribution of Underground Carbon Dioxide Salt Cavern Storage With State Space Model

Zhou Yuan [1,2†], Yanxi Zhou [1†], Minghui Wei [1*] and Xinwei Liao [2]

[1] School of Mechanical and Electrical Engineering, Southwest Petroleum University, Chengdu, China, [2] State Key Laboratory of Petroleum Resources and Prospecting, China University of Petroleum, Beijing, China

Underground salt caverns have become one of the potential methods for carbon dioxide (CO_2) storage due to its advantages including high storage capacity and easy construction. The wellbore and salt cavern heat transfer models for the CO_2 injection process was developed and solved by the state space method. This method can not only solve the partial differential equation, but can also be used as the basic model of automatic control. The results indicate that the temperature of annulus and the salt cavern are significantly influenced by the injection rate during the injection process, while the brine temperature in tubing remains almost unchanged. When the injection process stops, the temperature of annulus and the salt cavern are dominated by the formation temperature. The temperature of tubing brine mainly changes after a few hours, causing crystals to separate out from the brine, which can also explain why the tubing is blocked when the gas injection stops.
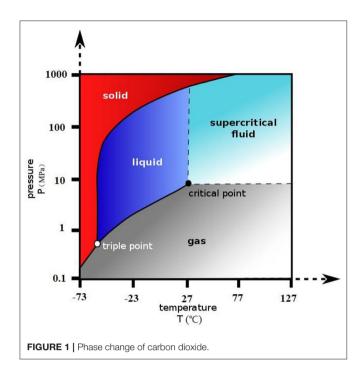
Keywords: salt cavern, CO_2 storage, heat transfer, state space method, injection process

INTRODUCTION

With the advent of industrial development, carbon dioxide (CO_2) has an increasingly high concentration in the atmosphere as a result of the combustion of fossil fuels, such as coal, petroleum, and natural gas, which has caused the rising trend in the Earth's average temperature. There are nearly 1.03×10^9 tons of CO_2 emissions in China every year (Li et al., 2017). How to deal with carbon dioxide emissions has become a global problem. Carbon capture and storage (CCS) is a technique of lower carbon utilization for fossil fuels on a large scale (Li et al., 2015). This technique was developed in the 1970s and has been used in enhanced oil recovery with CO_2 (CO_2-EOR), in enhanced geothermal systems with CO_2 (CO_2-EGS), CO_2 storage with gas recovery (CO_2-EGR), and CO_2 storage with saline water recovery (CO_2-EWR) (Wang et al., 2012; Sun et al., 2013; Boot-Handford et al., 2014; Li et al., 2014; Luo et al., 2014; Middleton et al., 2015; Wei et al., 2020). In recent years, a group of underground salt cavern storages with various advantages have been built in China (Zhang and Goh, 2012). Firstly, man-made salt caverns can be sized by specific demands by water-jet and the capacity of one salt cavern is usually $2–5 \times 10^5$ m³ (Bérest, 2019). Furthermore, using a salt cavern as CO_2 storage is different from traditional methods, where CO_2 can be drawn from all the time. Therefore, the salt cavern has extensive application properties for CO_2 storage (Kushnir et al., 2012).

The accurate prediction of wellbore and cavern temperature plays an important role in keeping the storage a safe and smooth process. It has great significance for judging the strength and

FIGURE 1 | Phase change of carbon dioxide.

stability of wellbore and salt caverns. For the underground salt cavern system, while the injection has stopped for a few hours, the crystal in tubing brine may separate out as the temperature changes, which would block the tubing, and affect the CO_2 storage system performance. What is more, when CO_2 approaches a supercritical state (31.1°C, 7.38 MPa) drastic change would occur somewhere along the wellbore and in the salt cavern, which would not be expected during the injection process (Li et al., 2017).

Studies on wellbore temperature distribution have been conducted since the 1950s. Both numerical and analytical approaches have been adopted to estimate the wellbore temperature (Hasan and Kabir, 1996; Wei et al., 2020). The earliest study of wellbore temperature was by Ramey. He drew charts for predicting bottom-hole circulating temperatures (Ramey, 1962; Wei et al., 2020) and proposed a steady-state model for obtaining the hole wellbore temperature distribution, which could not be applied to transient behavior (Hasan and Kabir, 2002; Yang et al., 2017; Wei et al., 2020). Raymond proposed the first numerical model for predicting temperature distributions for both transient and pseudo-steady-state conditions (Raymond, 1969). Hasan proposed the analytic methods for wellbore temperature prediction (Hasan et al., 1997, 1998). For CO_2 injection, the flow and thermal behavior in the wellbore involves some unique characteristics. Many researchers also developed CO_2 two-phase flow models under isothermal conditions (Wang et al., 2011a,b; Guo and Zeng, 2015; Li et al., 2016; Wei et al., 2020). Although using a salt cavern for CO_2 storage is not equal to injecting CO_2 into the wellbore. It needs to consider the heat transfer of annulus, tubing, and the salt cavern (Zhang and Goh, 2015; Wang et al., 2019. There have been few research topics that have focused on this field before (Kyuro and Yuichi, 2011; Goh and Zhang, 2012).

This study develops mathematical models to calculate the wellbore and salt cavern heat transfer models during CO_2 injection and injection-stopped periods, and models were solved by the state space method. This method can not only be used for solving partial differential equations, but also as an automatic control model. The results demonstrated that wellbore and cavern temperatures were significantly influenced by the injection rate during the injection process, and the tubing brine temperature had remained approximately constant. When the injection stopped, the wellbore and cavern temperatures were dominated by the formation temperature. The main variation in the tubing brine temperature occurred a few hours after the injection had stopped which would cause crystals to separate out from the brine. This is the reason why the tubing may be blocked after the injection process is stopped. The model can be used to design CO_2 injection parameters and monitor salt cavern states, and reduce the risk to the underground salt cavern system.

MATHEMATICAL MODEL

Figure 1 shows the phase change of CO_2, when CO_2 approaches the supercritical state (31.1°C, 7.38 MPa), which is likely to occur somewhere along the wellbore and in the salt cavern (Li et al., 2017; Wei et al., 2020).
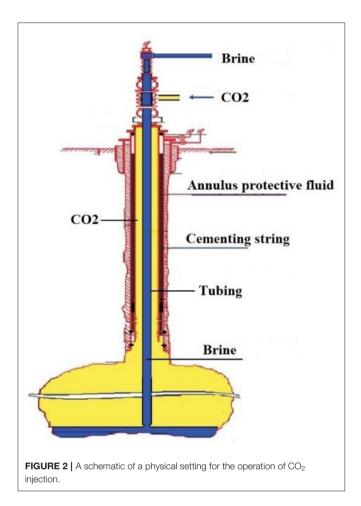
Figure 2 describes the process of injecting CO_2 into the salt cavern storage which can be divided into two parts. The first part: the fluid of CO_2 is injected into the salt cavern storage through annulus. The second part: the fluid of brine in the salt cavern storage flows through the tubing to the ground. Based on the principle of the conservation of energy, the dynamic mathematical model of heat transfer in the process of injecting CO_2 into the salt cavern storage is established (Wei et al., 2020).

The Heat Transfer Model of Annulus

According to **Figure 2**, in the CO_2 heat transfer model of annulus, the energy change is equal to the heat generated by the axial flow of CO_2, the heat transfer between the CO_2 of annulus and the tubing, and that between the well wall and the CO_2 of annulus. Therefore, the heat transfer model is Li et al. (2017) and Wei et al. (2020):

$$\rho_a A_a C_a \frac{\partial T_a}{\partial t} = -M_a C_a \frac{\partial T_a}{\partial z} + 2\pi r_1 \lambda_1 [T_f - T_a]$$
$$+2\pi r_2 \lambda_2 [T_w - T_a] \qquad (1)$$

where T_a is the annulus fluid temperature of CO_2, °C. T_w is the tubing temperature, °C. T_f is the well wall temperature, °C. ρ_a is the CO_2 density of annulus, kg/m^3. A_a is the area of annulus, m^2. C_a is the CO_2 specific heat of the annulus fluid, J/kg.°C. M_a is the mass flow of injected CO_2, kg/s. r_1 is the radius of annulus, m r_2 is the outer radius of tubing, m. λ_1 is the convective heat transfer coefficient of annulus CO_2 and the well wall, W/m$^{2.}$°C. λ_2 is the convective heat transfer coefficient of annulus CO_2 and tubing, W/m$^{2.}$°C.

FIGURE 2 | A schematic of a physical setting for the operation of CO_2 injection.

The Heat Transfer Model of Tubing Fluids

The fluid in the tubing is brine, the energy change of it is equal to the heat generated by the axial flow of the brine, and the heat exchange with the tubing brine and the tubing. Therefore, the heat transfer model is:

$$\rho_p A_p C_p \frac{\partial T_p}{\partial t} = \rho_p A_p C_p v_p \frac{\partial T_p}{\partial z} + 2\pi r_3 \lambda_3 [T_w - T_p] \quad (2)$$

where T_p is the tubing fluid temperature of brine, °C. ρ_p is the density of the tubing fluid, kg/m³. A_p is the area of the tubing, m². C_p is the specific heat of tubing brine, J/kg.°C. r_3 is the inner radius of tubing, m. v_p is the fluids flow velocity in the tubing, m/s. λ_3 is the convective heat transfer coefficient between the tubing brine and tubing, W/m².°C.

The Heat Transfer Model of Tubing

For the tubing, the energy change is equal to the convection heat transfer between the annulus CO_2 and the tubing, and that between the brine and the tubing. Therefore, the heat transfer model is:

$$\rho_w A_w C_w \frac{\partial T_w}{\partial t} = 2\pi r_2 \lambda_2 [T_a - T_w] + 2\pi r_3 \lambda_3 [T_p - T_w] \quad (3)$$

where ρ_w is the density of tubing, kg/m³. A_w is the area of tubing, m². C_w is the specific heat of tubing, J/kg°C.

Heat Transfer Model of Salt Cavern Storage

For the CO_2 which is stored in the salt cavern storage, the energy change is equal to the heat transfer between the CO_2 and the salt cavern storage wall, and that between the CO_2 and the brine in the salt cavern storage, and the energy entered from the annulus. Therefore, the heat transfer model is:

$$m_c C_c \frac{\partial T_c}{\partial t} = A_{f1} \lambda_{f1} \left[T_{fc} - T_c \right] + A_c \lambda_{bc} \left[T_b - T_c \right]$$
$$+ M_a C_c \left[T_{ab} - T_c \right] \quad (4)$$

where, T_c is a cavern's CO_2 temperature, °C. T_{fc} is a cavern's formation temperature, °C. T_b is the brine in the salt cavern storage temperature, °C. T_{ad} is the CO_2 temperature that flows into the cavern from the annulus, °C. m_c is the CO_2 quality in the salt cavern storage, kg. C_c is the CO_2 heat capacity in the salt cavern storage, J/kg.°C. A_{f1} is the contact area of the CO_2 and the salt cavern storage wall, m². A_c is the contact area of the brine in the salt cavern storage and the CO_2 in the salt cavern storage, m². λ_{f1} is the heat transfer coefficient between the CO_2 and the salt cavern storage wall, W/m².°C. λ_{bc} is the heat transfer coefficient between the CO_2 and the brine in the salt cavern storage, W/m².°C. M_a is the mass flow rate of injected gas, kg/s. T_{ad} is the temperature of the CO_2 which is injected into the salt cavern storage from annulus, °C.

The brine energy change in the salt cavern storage is equal to the heat transfer between brine and the salt cavern wall, and that between the brine and the CO_2. Therefore, the heat transfer model is:

$$m_b C_b \frac{\partial T_b}{\partial t} = A_{f2} \lambda_{f2} \left[T_f - T_b \right] + A_c \lambda_{cb} \left[T_c - T_b \right] \quad (5)$$

where, m_b is the quality of brine in the salt cavern storage, kg. C_b is the heat capacity of the brine in the salt cavern storage, J/kg.°C. A_{f2} is the contact area of the brine and the salt cavern storage wall, m². A_c is the contact area of the CO_2 in the salt cavern and the brine in the salt cavern, m². λ_{f2} is the heat transfer coefficient of the brine and the salt cavern storage wall, W/m².°C. λ_{cb} is the heat transfer coefficient of the brine and CO_2 in the salt cavern storage, W/m².°C.

INITIAL CONDITION AND BOUNDARY CONDITION AND STATE-SPACE METHOD FOR THE WELLBORE

In the process of gas injection, mass flow and injection temperature is measured on the ground. The formation temperature is attained using the surface temperature and the formation temperature gradient, the formation temperature gradient is 3°C/100 m, thus $T_f = T_{f0} + yz$, T_{f0} is the formation

temperature, y is the formation temperature gradient, and z represents depth.

The state space method is a basic model of modern control theory. So it can not only solve the partial differential equation, but can also be used as the basic model of automatic control.

For Equations (1–4), using difference instead of integral, therefore:

$$\frac{\partial T}{\partial t} = \frac{T(k+1,1) - T(k,1)}{\Delta t} \quad \frac{\partial T}{\partial z} = \frac{T(1,j) - T(1,j-1)}{\Delta z}$$

(6)

Equation (1) can be expressed as:

$$\rho_a A_a C_a \frac{T_a(k+1,j) - T_a(k,j)}{\Delta t} = -M_a C_a \frac{T_a(k,j) - T_a(k,j-1)}{\Delta z}$$
$$+ 2\pi r_2 \lambda_2 \left[T_w(k,j) - T_a(k,j) \right] + 2\pi r_3 \lambda_3 \left[T_f(k,j) - T_a(k,j) \right]$$

(7)

The depth of wellbore is divided into L nodes, each discrete time is represented by k, according to the linear system theory, each grid temperature in the tubing and annulus is an independent state. Set the gas injection temperature as $T_a(k,0)$, and set $x_1 = -\frac{M_a \Delta t}{\rho_a A_a \Delta z}$, $x_2 = \frac{2\pi r_2 \lambda_2 \Delta t}{\rho_a A_a C_a}$, $x_2 = \frac{2\pi r_3 \lambda_3 \Delta t}{\rho_a A_a C_a}$, and the state space model for the wellbore heat transfer system can be obtained. Equation (1) converts to Wei et al. (2020):

$$T_A(k+1) = A_a T_A(k) + B_a T_W(k) + C_a T_F(k) + D_a U_d(k) \quad (8)$$

where,

$$T_A(k) = \left[T_a(k,1), T_a(k,2), T_a(k,3), \cdots T_a(k,L) \right]_{L \times 1}^T$$
$$T_W(k) = \left[T_w(k,1), T_w(k,2), T_w(k,3), \cdots T_w(k,L) \right]_{L \times 1}^T$$
$$T_F(k) = \left[T_f(k,1), T_f(k,2), T_f(k,3), \cdots T_f(k,L) \right]_{L \times 1}^T$$
$$U_d(k) = \left[T_a(k,0), 0, 0, \cdots 0 \right]_{L \times 1}^T$$

$$A_a = \begin{bmatrix} x_1 + 1 - x_2 - x_3 & 0 & 0 & \cdots & & 0 \\ -x_1 & x_1 + 1 - x_2 - x_3 & 0 & \cdots & & 0 \\ 0 & -x_1 & \ddots & \ddots & & 0 \\ \vdots & 0 & \ddots & x_1 + 1 - x_2 - x_3 & 0 \\ 0 & 0 & 0 & -x_1 & x_1 + 1 - x_2 - x_3 \end{bmatrix}_{L \times L}$$

$$B_a = x_2, C_a = x_3, D_a = -x_1$$

where, T_A is the state vector of the heat transfer state space model for annulus fluid of CO_2, T_W is the state vector of tubing temperature, T_F is the state vector of formation temperature, U_d is the input vector for the state space model, and A_a is the system matrix. In the same way, set $z_1 = -v_p \frac{\Delta t}{\Delta z}$, $z_2 = \frac{2\pi r_1 \lambda_1 \Delta t}{\rho_P A_P C_P}$, and the brine temperature from the cavern that entered into the tubing as $T_p(k,0)$, we can get the state space model of the brine temperature in the tubing (Wei et al., 2020).

$$T_P(k+1) = A_P T_P(k) + B_P T_W(k) + D_P U_P(k) \quad (9)$$

where,

$$T_P(k) = \left[T_P(k,1), T_P(k,2), T_P(k,3), \cdots T_P(k,L) \right]_{L \times 1}^T$$
$$T_W(k) = \left[T_w(k,1), T_w(k,2), T_w(k,3), \cdots T_w(k,L) \right]_{L \times 1}^T$$
$$U_P(k) = \left[T_P(k,0), 0, 0, \cdots 0 \right]_{L \times 1}^T$$
$$A_p =$$
$$\begin{bmatrix} z_1 + 1 - z_2 & 0 & 0 & \cdots & & 0 \\ -z_1 & z_1 + 1 - z_2 & 0 & \cdots & & 0 \\ 0 & -z_1 & \ddots & \ddots & & 0 \\ \vdots & 0 & \ddots & z_1 + 1 - x_2 & 0 \\ 0 & 0 & 0 & -z_1 & z_1 + 1 - z_2 \end{bmatrix}_{L \times L}$$

$$B_a = z_2, D_a = -z_1$$

where, T_P is the state vector of the heat transfer state-space model for the tubing fluid of brine, U_p is the input vector, and A_p is the system matrix.

Salt cavern storage temperature state space model:

Set $y_1 = \frac{A_{f1} \lambda_{f1} \Delta t}{m_c C_c}$, $y_2 = \frac{A_c \lambda_{bc} \Delta t}{m_c C_c}$, $y_3 = \frac{M_a C_c \Delta t}{m_c C_c}$, $z_1 = \frac{A_{f2} \lambda_{f2} \Delta t}{m_b C_b}$, $z_2 = \frac{A_c \lambda_{cb} \Delta t}{m_b C_b}$, So (3), (4) can be transformed into the state space model for calculating the temperature of gas and brine in salt cavern storage

$$\begin{bmatrix} T_c(k+1) \\ T_b(k+1) \end{bmatrix} = \qquad (10)$$
$$\begin{bmatrix} 1 - y_1 - y_2 - y_3 & y_3 \\ z_2 & 1 + z_1 + z_2 \end{bmatrix} \begin{bmatrix} T_c(k) \\ T_b(k) \end{bmatrix} + \begin{bmatrix} y_1 & 1 \\ z_1 & 0 \end{bmatrix} \begin{bmatrix} T_f \\ T_{ad} \end{bmatrix}$$

The CO_2 gas in the salt cavern storage satisfies the gas equation. Before calculation, the initial density of gas in the salt cavern storage can be calculated according to the initial pressure of the gas in the salt cavern storage and the gas state equation.

$$\rho_c = \frac{P_c M}{8.314 Z T_c} \qquad (11)$$

where M is the molecular mass of natural gas, and Z is the pressure factor, which can be obtained by:

$$Z = 0.702 e^{-2.5 T_r} p_r^2 - 5.524 e^{-2.5 T_r} p_r \qquad (12)$$
$$+ \left(0.044 T_r^2 - 0.164 T_r + 1.15 \right)$$

$$p_r = \frac{p}{p_e}, T_r = \frac{T}{T_e} \qquad (13)$$

Parameter	Value	Parameter	Value
Well depth, m	500	Mass flow rate, kg/s	16
Tubing inner diameter, mm	100	Initial injection pressure, MPa	5
Tubing outer diameter, mm	114	Injection temperature, °C	21
Well-bore diameter, mm	178	Surface earth temperature, °C	20
Salt cavern volume, m^3	2×10^5	Brine density, kg/m^3	1,200
Salt cavern's sectional area, m^2	2,500	Salt cavern's height, m	80
Thermal conductivity of formation, W/m.°C	0.52	Thermal conductivity of tubing, W/m.°C	44.7
Thermal conductivity of Salt cavern, W/m.°C	0.08		

where Pr is the pseudo-reduced pressure, dimensionless; Tr is the pseudo-reduced temperature, dimensionless; Pc is the critical pressure of CO_2 gas, Pa; Tc is the critical temperature of gas, K (Ren et al., 2016).

After every step, the mass of CO_2 gas in the cavern is:$m_c(k+1) = M_a\Delta t + m_c(k)$. The density of natural gas in the cavern is:

$$\rho_c(k) = m_c(k)/V_c \qquad (14)$$

According to Equations (11–14), the pressure of the cavern can be obtained. To ensure that the carbon dioxide in the salt cavern storage will not have a phase change, the allowed pressure of the cavern is generally <7 MPa.

CASE STUDY

The state space model was used to show the transient temperature distribution of underground CO_2 salt cavern storage, supposing the salt cave's shape is cylindrical and its simulation data were shown in **Table 1** (Zhang and Goh, 2012; Bérest, 2019).
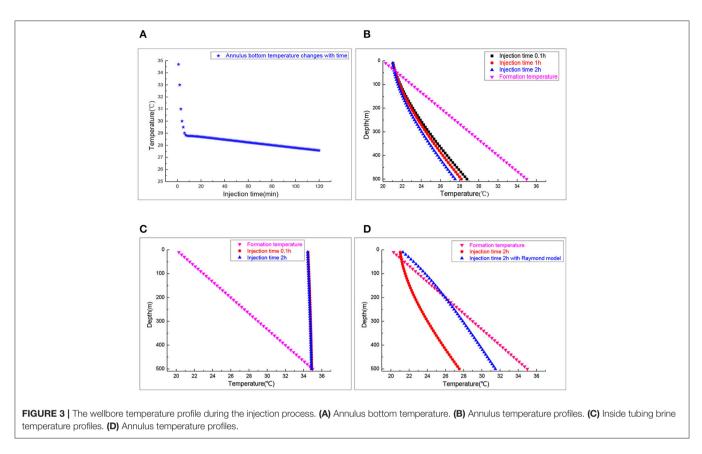
The wellbore temperature profiles, as a function of well depth under different injection times, are calculated by the state space method. As shown in **Figure 3A**, the temperature decreases with injection and reaches a quasi-stable state temperature of 27.5°C at the bottom of annulus. The time needed to reach the quasi steady state is about 20 min. Therefore, special attention should be paid to monitoring in the first 20 min during the injection process. **Figure 3B** signifies the annulus temperature profiles after injection for 0.1, 1, and 2 h. With the increase of injection time, the annulus temperature decreases, its temperature variation is 1.5°C at the bottom of the annulus. **Figure 3C** manifests the effect of different gas injection times on the brine temperature distribution in the tubing. The steady state temperature of the tubing brine remains almost unchanged at two injection times. Therefore, the crystal separating out from brine due to the temperature changes would not occur during the injection process.
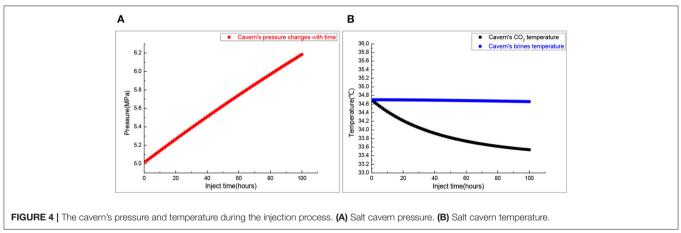
The tubing heat transfer effect was neglected in the Raymond model while tubing's influence on temperature distribution of the annulus was considered in the state space model. The material of the tubing used is steel which is used in petroleum and matches the American Petroleum Institute (API) specifications. **Figure 3D** displays the tubing heat transfer effect on the annulus temperature distribution. More heat would enter the annulus from the formation transferring without considering it. The annulus CO_2 temperature calculated by the Raymond model is about 3–4°C lower than that by the state space model. Therefore, when calculating the annulus CO_2 temperature, the influence of tubing heat transfer could not be ignored.

Figure 4 presents the change of the salt cavern temperature and pressure during the injection process. The pressure prediction is also very important for stable operation of the gas storage. For salt cavern gas storage, the general pressure range is about 5–25 MPa. As shown in **Figure 4A**, salt cavern pressure increases from 5 to 6.1 MPa in an 80-h injection. It is in the allowable operating pressure range. **Figure 4B** shows the temperature variation of salt cavern CO_2 and brine in a 60-h injection, and CO_2 temperature decreases to a new quasi-steady state. According to **Figure 1**, there is no CO_2 phase change during the injection process so it meets the design requirement. We can calculate that the CO_2 mass is 1.9978×10^7 Kg.

Figure 5 is the effect of the gas injection rate on CO_2 storage system operation state. **Figure 5A** demonstrates the annulus CO_2 temperature profiles in CO_2 injection rates of 13, 16, and 20 kg/s. Different CO_2 injection rates have little influence on the annulus temperature above 100-m depth. The annulus temperature in the middle and lower part gradually decreased with the increased injection rate. **Figure 5B** shows the temperature variation of the brine in the tubing. When the CO_2 injection rate changed, the brine temperature changed very little. **Figure 5C** manifests the CO_2 gas pressure in the salt cavern at different CO_2 injection rates. When the CO_2 injection rates were 13, 16, and 20 kg/s, the CO_2 gas pressure in the salt cavern was 5.9, 6.1, and 6.4 MPa, respectively, after an 100-h CO_2 injection. The CO_2 gas pressure in the salt cavern increased significantly with the increase of the gas injection rate. **Figure 5D** shows the variation of CO_2 gas temperature in the salt cavern at different injection rates. As the injection rate increased, the CO_2 gas temperature in the salt cavern decreased significantly, and reached new and different quasi-steady states.

Figure 6 is the change of the temperature in the wellbore and salt cavern when the well was shut in. **Figure 6A** signifies the change of CO_2 gas temperature in the salt cavern storage when the well was shut in. During the injection process, the temperature of injection CO_2 plays a dominant role in the salt cavern's temperature. When CO_2 injection stops, the heat transfer between the formation and salt cavern's CO_2 plays a dominant role in the salt cavern's temperature. The CO_2 gas temperature in the salt cavern storage increases after the well is shut in, but the increasing trend slows and gradually approaches the formation temperature. **Figure 6B** shows the change of CO_2 gas pressure in salt cavern storage when the well is shut in. When the well was shut in, the CO_2 gas
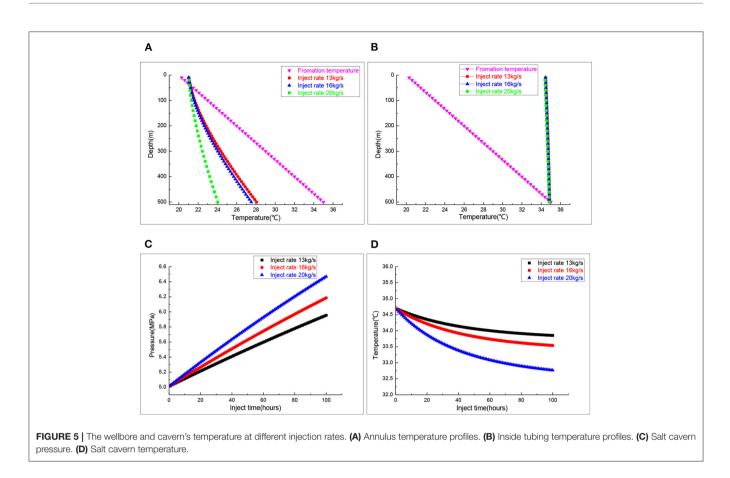
FIGURE 3 | The wellbore temperature profile during the injection process. **(A)** Annulus bottom temperature. **(B)** Annulus temperature profiles. **(C)** Inside tubing brine temperature profiles. **(D)** Annulus temperature profiles.

FIGURE 4 | The cavern's pressure and temperature during the injection process. **(A)** Salt cavern pressure. **(B)** Salt cavern temperature.

pressure in salt cavern storage changes with the temperature change, but the change is very small. **Figure 6C** shows the distribution of annulus CO_2 temperature at different time points when the well is shut in. Due to the heat transfer between the formation and the brine in the tubing, the annulus temperature firstly increases and then decreases. At first, the annulus temperature is lower than the formation temperature, then it becomes higher than it, and finally approaches the current formation temperature. **Figure 6D** shows the brine temperature in the tubing in 1, 5, and 20 h after the well was shut in, and the brine temperature in the tubing gradually approached

the formation temperature. The result shows that heat transfer between the wellbore and formation play a dominant role in the brine temperature distribution in the tubing after the well is shut in.

Figure 7 shows the distribution of the temperature variation between the temperature when the well was shut in for 20 h and the temperature just after gas injection was stopped. The change of brine temperature in the tubing mainly occurs when the well was shut in. The change of temperature will cause crystals to separate out from the brine, which can explain the blockage of the tubing when the well was shut in.
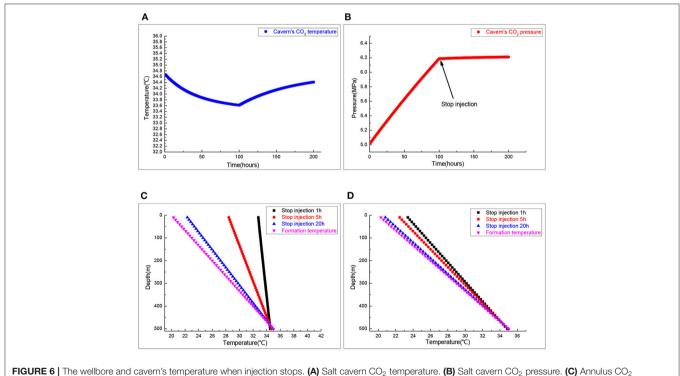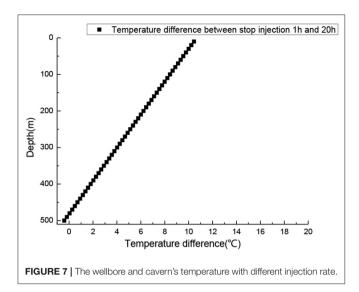
FIGURE 5 | The wellbore and cavern's temperature at different injection rates. **(A)** Annulus temperature profiles. **(B)** Inside tubing temperature profiles. **(C)** Salt cavern pressure. **(D)** Salt cavern temperature.

FIGURE 6 | The wellbore and cavern's temperature when injection stops. **(A)** Salt cavern CO_2 temperature. **(B)** Salt cavern CO_2 pressure. **(C)** Annulus CO_2 temperature profiles. **(D)** Inside tubing brine temperature.

FIGURE 7 | The wellbore and cavern's temperature with different injection rate.

CONCLUSION

This thesis proposes a new method (using underground salt cavern storage) for CO_2 storage and a mathematical model for transient temperature distribution during the CO_2 injection process. Furthermore, state space method is used for solving this model, where CO_2 storage's temperature-pressure can be predicted, and parameters of CO_2 storage can be monitored and optimized during the CO_2 injection process.

The operating parameters analysis manifests that flow rates have a significant impact on the temperature of the wellbore and the cavern. In addition, when the injection is stopped, heat transfer is dominated by the formation temperature, resulting in a remarkable increase in annulus temperature. The temperature of tubing brine mainly changes when injection stops, which is very important in preventing blockages in the tubing.

This research may help interpret the mechanism of wellbore and cavern heat transfer during CO_2 injection. This heat transfer model of wellbore and cavern is our primary work. Future work will be focused on the CO_2 releasing process and the phase variation in the process.

DATA AVAILABILITY STATEMENT

The raw data supporting the conclusions of this article will be made available by the authors, without undue reservation.

AUTHOR CONTRIBUTIONS

ZY and YZ: stimulation, data curation, and writing manuscript. MW: construction of thesis ideas, establish mathematical model, and provide research fund. XL: manuscript review. All authors contributed to the article and approved the submitted version.

REFERENCES

Bérest, P. (2019). Heat transfer in salt caverns. *Int. J. Rock Mech. Rock Eng. Min. Sci.* 120, 82–95. doi: 10.1016/j.ijrmms.2019.06.009

Boot-Handford, M., Abanades, J. C., Anthony, E., Blunt, M., and Brandani, S. (2014). Carbon capture and storage update. *Energy Environ. Sci.* 7, 130–189. doi: 10.1039/C3EE42350F

Goh, A. T., and Zhang, W. (2012). Reliability assessment of stability of underground rock caverns. *Int. J. Rock Mech. Mining Sci.* 55, 157–163. doi: 10.1016/j.ijrmms.2012.07.012

Guo, J., and Zeng, J. (2015). A coupling model for wellbore transient temperature and pressure of fracturing with supercritical carbon dioxide. *Shi You XueBao/ActaPet. Sin.* 36, 203–209. doi: 10.7623/syxb20 1502009

Hasan, A. R., and Kabir, C. S. (1996). A mechanistic model for computing fluid temperature profiles in gas-lift wells. *SPE Prod. Facil.* 11, 179–185. doi: 10.2118/26098-PA

Hasan, A. R., and Kabir, C. S. (2002). *Fluid Flow and Heat Transfer in Wellbores.* Richardson, TX: SPE.

Hasan, A. R., Kabir, C. S., and Wang, X. (1997). *Development and Application of a Wellbore/Reservoir Simulator for Testing Oil Wells.* SPEFE.

Hasan, A. R., Kabir, C. S., and Wang, X. (1998). *Wellbore Two-Phase Flow and Heat Transfer During Transient Testing.* SPEJ.

Kushnir, R., Dayan, A., and Ullmann, A. (2012). Temperature and pressure variations within compressed air energy storage caverns. *Int. J. Heat Mass Transfer* 55, 5616–5630. doi: 10.1016/j.ijheatmasstransfer.2012. 05.055

Kyuro, S., and Yuichi, S. (2011). Heat Transfer and Phase Change in Deep CO2 Injector for CO2 Geological Storage. *Two Phase Flow, Phase Change and Numerical Modeling.* Fukuoka: InTech.

Li, Q., Wei, Y. N., Liu, G., and Lin, Q. (2014). Combination of CO_2 geological storage with deep saline water recovery in western China: insights from numerical analyses. *Appl. Energy* 116, 101–110. doi: 10.1016/j.apenergy.2013.11.050

Li, X., Li, G., Wang, H., Lu, P., Tian, S., and Song, X. (2017). A unified model for wellbore flow and heat transfer in pure CO_2 injection for geological sequestration, EOR and fracturing operations. *Int. J. Greenhouse Gas Control* 42, 602–614. doi: 10.1016/j.ijggc.2016.11.030

Li, X., Li, G., Wang, H., Lu, P., Tian, S., Yang, R., et al. (2016). "A coupled model for predicting flowing temperature and pressure distribution in drilling ultra-short radius radial wells," in *IADC/SPE Asia Pacific Drilling Technology Conference,* (Singapore), 22–24.

Li, X., X, R., Wei, L., and Jiang, P. (2015). Modeling of wellbore dynamics of a CO2 injector during transient well shut-in and start-up operations. *Int. J. Greenhouse Gas Control* 42, 602–614. doi: 10.1016/j.ijggc.2015.09.016

Luo, F., Xu, R. N., and Jiang, P. X. (2014). Numerical investigation of the doublet enhanced geothermal system with CO2as working fluid (CO2-EGS). *Energy* 64, 307–322. doi: 10.1016/j.energy.2013.10.048

Middleton, R. S., Carey, J. W., Currier, R. P., Hyman, J. D., Kang, Q., Karra, S., et al. (2015). Shale gas and non-aqueous fracturing fluids: opportunities and challenges for supercritical CO_2. *Appl. Energy* 147, 500–509. doi: 10.1016/j.apenergy.2015.03.023

Ramey, H. J. (1962). Wellbore heat transmission. *J. Pet. Technol.* 14, 427–435. doi: 10.2118/96-PA

Raymond, L. R. (1969). Temperature distribution in a circulating drilling fluid. *J. Pet. Technol.* 21, 333–341. doi: 10.2118/2320-PA

Ren, W., Li, G., Tian, S., Sheng, M., and Fan, X. (2016). An analytical model for real gas flow in shale nanopores with non-circular cross-section. *AIChE J.* 62, 2893–2901. doi: 10.1002/aic.15254

Sun, H., Yao, J., Gao, S. H., Fan, D. Y., Wang, C. C., and Sun, Z. X. (2013). Numerical study of CO_2 enhanced natural gas recovery and sequestration in shale gas reservoirs. *Int. J. Greenh. Gas Control* 19, 406–419. doi: 10.1016/j.ijggc.2013.09.011

Wang, H., Li, G., and Shen, Z. (2012). A feasibility analysis on shale gas exploitation with supercritical carbon dioxide. *Energy Sources Part A* 34, 1426–1435. doi: 10.1080/15567036.2010.529570

Wang, H., Shen, Z., and Li, G. (2011a). Influences of formation water invasion on the wellbore temperature and pressure in supercritical CO_2 drilling. *Pet. Explor. Dev.* 38, 362–368. doi: 10.1016/S1876-3804(11)60039-6

Wang, H., Shen, Z., and Li, G. (2011b). Wellbore temperature and pressure coupling calculation of drilling with supercritical carbon dioxide. *Pet. Explor. Dev.* 38, 97–102.

Wang, Z., Wang, L., and Zhang, W. (2019). A random angular bend algorithm for two- dimensional discrete modeling of granular materials. *Materials.* 12:2169. doi: 10.3390/ma12132169

Wei, M., Wu, C., and Zhou, Y. (2020). Study on wellbore temperature and pressure distribution in process of gas hydrate mined by polymer additive CO_2 jet. *Adv. Polymer Technol.* 2020, 1–7. doi: 10.1155/2020/2914375

Yang, M., Zhao, X., and Meng, Y. (2017). Determination of transient temperature distribution inside a well bore considering drill string assembly and casing program. *Appl. Thermal Eng.* 118, 299–314. doi: 10.1016/j.applthermaleng.2017.02.070

Zhang, W., and Goh, A. T. (2012). Reliability assessment on ultimate and serviceability limit states and determination of critical factor of safety for underground rock caverns. *Tunnel. Undergr. Space Technol.* 32, 221–230. doi: 10.1016/j.tust.2012.07.002

Zhang, W. G., and Goh, A. T. C. (2015). Regression models for estimating ultimate and serviceability limit states of underground rock caverns. *Eng. Geol.* 188, 68–76. doi: 10.1016/j.enggeo.2015.01.021